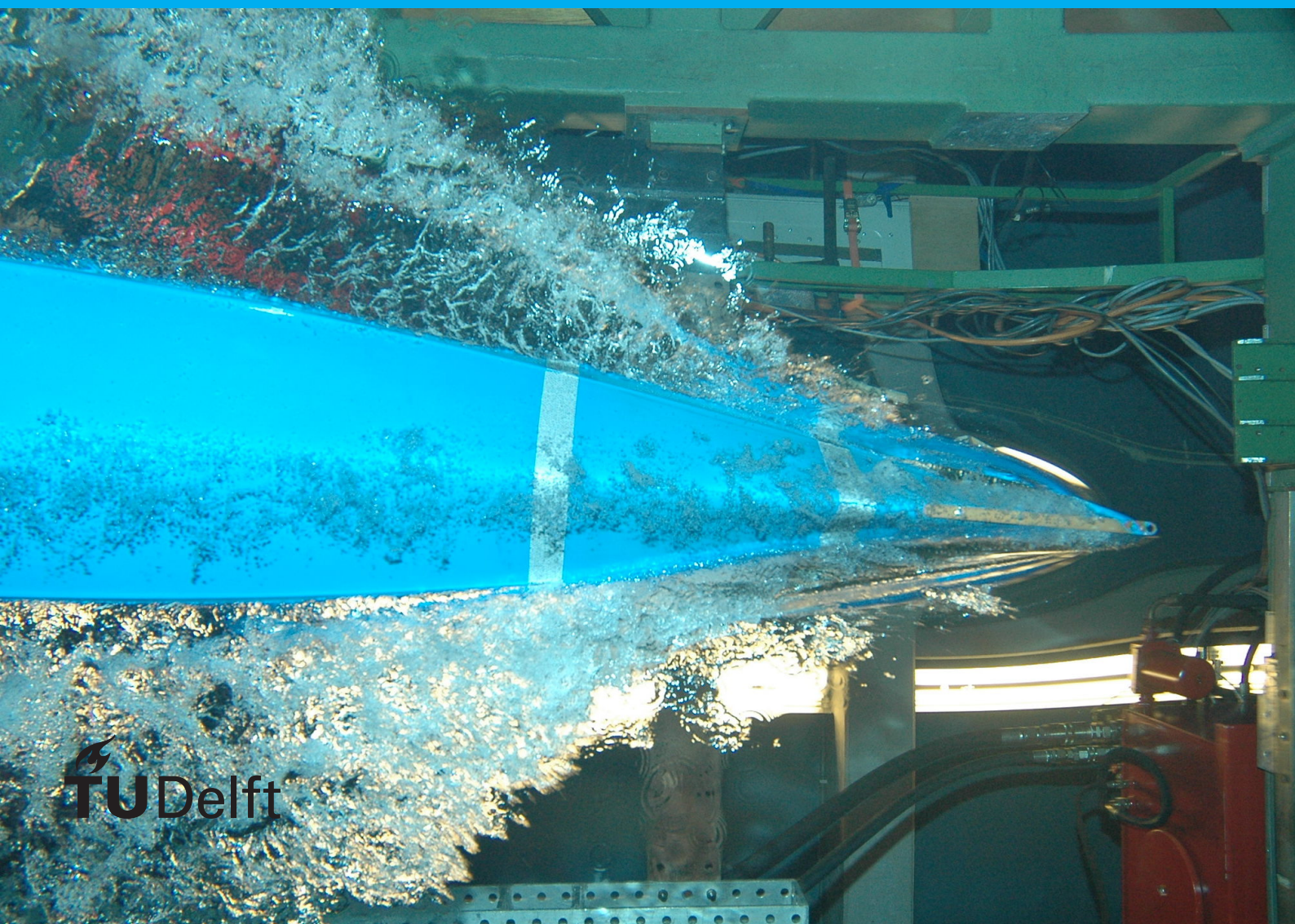


Inversion of magnetic data for unexploded Ordnance (UXO) detection

Anna Flouri



Inversion of magnetic data for unexploded Ordnance (UXO) detection

by

Anna Flouri

to obtain the degree of Master of Science
at the Delft University of Technology,
to be defended publicly on Tuesday August 20, 2021 at 12:00 PM.

Student number: 5155630
Project duration: March 1, 2021 – August 6, 2021
Thesis committee: Prof. Dr. Ir. E.C. Slob, TU Delft, supervisor
M. Künzel, League Geophysics
Dr. Ir. D.S. Draganov, TU Delft
Dr. Ir. Dirk-Jan van Manen, ETH Zürich

An electronic version of this thesis is available at <http://repository.tudelft.nl/>.

Symbols

J [A/m^2] Current density
 ρ [Cm^3] Charge Density
B [nT] Magnetic Field Flux
H [A/m] Magnetic field intensity
 μ_o / μ [H/m] magnetic permeability of the vacuum / material
 μ_r [-] relative permeability
M [A/m] Magnetization
 ϕ_p [A] Magnetic Scalar Potential
A [Tm] Magnetic Vector Potential
K [A/m] Surface Current Density
 \hat{n} Normal Unit Vector
x [m] observation point coordinates
x' [m] source coordinates
 x_o' [m] coordinates at the center of the source
r m distance between the center of the source and the observation point
V [m^3] Volume that contains the observation point
V' Volume of the source
S [m^2] Surface area that contains the observation point
S'[m^2] surface area of the source
 χ [-] volume magnetic susceptibility
m [A/m^2] magnetic moment
 b_o [nT] Geomagnetic Field
 b_s [nT] Magnetic Field of the spheroid
 b_{tot} [nT] Total Magnetic field
 b_a [nT] Total Magnetic Field Anomaly
 b_{a_z} [nT/m] Vertical Gradient Field
F [-] Demagnetization factors
e [-] aspect ratio
 α [m] diameter
R Rotation Matrix
 $\phi, \theta, \psi^{[o]}$ Rotation angles
m model parameters
f(m') objective function
Bolt letters denote vectors.

Abstract

The magnetic method is one of the geophysical techniques that prevails in the detection and identification of Unexploded Ordnance (UXO). Inversion of the magnetic data, allows us to recover the position and the magnetic dipole moment of the object. The typical use of a model is a sphere, though it does not provide information about the shape of the object. This thesis focuses on modeling a prolate spheroid, that not only recovers the position and the magnetic moment moment, but also the orientation and the dimensions of body. The results were fairly similar, though the residuals in the case of the sphere were less than the ones of the spheroid. In addition, measurements of real UXOS were used to verify the code. The inversion yielded reasonable models in four cases, but did not manage to recover an accurate model for one them. Lastly, the octupole moment was modeled as well, though its contribution to the results was deemed negligible.

Acknowledgements

I would like to thank the League Geophysics team for the help and the tools they provided in order for me to complete my thesis, especially my main supervisor Michiel Künzel. Special thanks to my academic supervisor Prof. Dr. Ir. E.C Slob for his valuable input and guidance with regards not only my thesis, but also with the general scientific research ideology.

Contents

Symbols	i
Abstract	ii
Acknowledgements	iii
1 INTRODUCTION	1
2 Theory	3
2.1 INDUCED MAGNETIZATION	5
2.2 DEMAGNETIZING FIELDS.	5
2.3 MULTIPOLE EXPANSION	7
2.3.1 MODELLING AN ELLIPSOID	8
3 FORMULATION OF THE PROBLEM	10
3.1 INVERSION.	10
3.2 INVERSION METHOD	10
3.2.1 BUILDING THE CODE	11
3.3 SYNTHETIC RESULTS	13
4 REAL RESULTS	16
4.1 RIVER VERIFICATION TRIAL.	16
4.1.1 COMPARISON WITH SPHERE	16
4.2 REASEURO DATA	18
4.2.1 UNCERTAINTIES	19
4.2.2 HAND GRENADE.	19
4.2.3 CANNON BALL	20
4.2.4 MORTAR	21
4.2.5 BRITISH SHELL.	22
4.3 INVERSION RESULTS USING THE DIPOLE AND THE OCTUPOLE FIELD.	23
5 DISCUSSION AND CONCLUSIONS	26
A APPENDIX A	28

1

INTRODUCTION

Over the recent years, there has been an increasing amount of instances where Unexploded Ordnance (UXO) has caused severe injuries or death in citizens. Unexploded ordnances are mostly remnants of war, ammunition that did not detonate as intended. Sometimes they are not directly connected to war; for example in places where bombs were disposed or old military training bases. The need for location and extraction of UXO rises from the fact that such explosive remnants of war can spontaneously detonate or be set off, even years after their disposal.

According to UNICEF [1] , 78 countries suffer from land mines that kill or impair 15000-20000 people yearly. Even if UXO do not detonate, it is still essential that they are found, considering the negative effects they inflict on the environment. Toxic residue that infiltrates the water, the soil and air, might incite greater health issues than the actual explosion [2]. The unexpected presence of UXO in (offshore) construction works may also result in large additional costs and time in recovering these items. For offshore identification and removal, costs are around 150,000 euro per day and total costs on UXO removal on an offshore project may be several million euro (League Geophysics, pers.comm.)

Reliable geophysical methods for detecting UXO are therefore needed. The magnetic method is the most commonly used geophysical survey method for detecting UXO, both on land and under water. The method is fast and cheap and capable of detecting most ferromagnetic UXO, assuming that the environment is not polluted with magnetic noise and the height of the measurement is small enough to detect smaller objects. Electromagnetic methods are also used in conjunction with magnetic methods. Gravity measurements can provide information about the mass of the object, but their use is limited in small areas, while GPR can detect smaller objects but their use is limited in larger areas [3].

Reliably interpreting such magnetic data sets is the biggest challenge in modern UXO surveying. Industry standard software tends to be outdated and closed-source, leading to difficulties in reliable interpretation.

One of the major issues with the interpretation of the magnetic data is their non-uniqueness. That means that each anomaly can be produced by more than one object with different physical as well as geometrical characteristics. Modelling a UXO is challenging because they are defined by a wide range of properties that depend on the type, the way they are made as well as the decade that they have been manufactured.

One of the magnetic characteristics of the objects that has been recently used for the identification and discrimination of UXOs, is the magnetic dipole moment. The magnetic moment contains information about the intensity of magnetization, though it does not offer details about the shape [4]. The simplest model that someone can use is the sphere, a model that rarely represents an explosive. On the other hand an elongated sphere could likely be more close to the shape of a UXO. A number of publications are dedicated in utilizing prolate spheroid model for UXO objects. Mcfee et al. 1989 focused more on the physics and Billings et al. 2002 and Butler et al. 2012 applied the physics to real

situations. In addition, Butler et al.2012 investigated smaller objects in smaller distances and how the higher order terms affected his results.

League Geophysics is a start-up geophysical company, specialized in processing and interpreting geophysical data sets for UXO detection. Thus, this research will try to help them in increasing reliability of magnetic modelling for UXO interpretation, by:

1) Modelling and inverting for an axially-symmetric-prolate spheroid, as well as recovering the dipole moment, the location and the dimensions of the body.

2) Focusing primarily on the dipole field, though investigation of the contribution of the octupole will also occur.

3) Lastly, considering all the above, the final results will determine whether a spheroid model is better than a spherical model. Since the unknowns are seven and the code is using a gradient non-linear solver, the main challenges will be the choice of initial values, the effect of the remanent magnetization that is not accounted for, as well as dealing with the trade-off between a good fit and a reasonable model. Analysis of the theory, the code and its limitations will be discussed in the following chapters.

2

Theory

Moving charges constitute electric current that consequently will create magnetic field. If the current has steady flow, namely there is no accumulation of charge, then the time change of the charge density ρ is zero. Following the continuity theorem,

$$\nabla \cdot \mathbf{J} = -\frac{\partial \rho}{\partial t}, \quad (2.1)$$

where \mathbf{J} is the current density. Since the right hand side is zero, then $\nabla \cdot \mathbf{J} = 0$. The aforementioned relationship represents the basis for the domain of Magnetostatics.

The magnetic field flux \mathbf{B} accounts for the amount of magnetic field lines passing through a unit area, while the magnetic field intensity \mathbf{H} measures how strong the \mathbf{B} is at a certain point. They are described by:

$$\mathbf{B} = \mu_o \mathbf{H} \quad (2.2)$$

where μ_o is the magnetic permeability of the vacuum. If we assume a magnetic material with magnetic permeability μ then equation (2.2) becomes

$$\mathbf{B} = \mu \mathbf{H}, \quad (2.3)$$

or

$$\mathbf{B} = \mu_o (\mathbf{M} + \mathbf{H}), \quad (2.4)$$

where \mathbf{M} represents the magnetization of the object. A quick rearrangement of the terms will result in

$$\mathbf{M} = \mu_o^{-1} \mathbf{B} - \mathbf{H}. \quad (2.5)$$

If instead of μ we choose the relative permeability $\mu_r = \frac{\mu}{\mu_o}$, then

$$\mathbf{B} = \mu_r \mu_o \mathbf{H}. \quad (2.6)$$

The last step concerns the substitution of (2.6) in (2.5) which leads to

$$\mathbf{M} = (\mu_r - 1) \mathbf{H}. \quad (2.7)$$

[5].

The Helmholtz theorem states that a decaying vector field can be decomposed into a scalar field (scalar potential) and a vector field (vector potential).

$$\mathbf{B} = -\nabla \phi_p + \nabla \times \mathbf{A} \quad (2.8)$$

According to Gauss's law for the magnetic fields (and one of Maxwell's equations), there are no sources or sinks that cause the magnetic field. In other words, magnetic monopoles do not exist which explains the primary use of dipoles. Thus, $\nabla \cdot \mathbf{B} = 0$ and the scalar potential cannot be invoked. The first term of equation (2.8), becomes zero and the magnetic field can be expressed in terms of only vector potential ([6]).

An additional important law is Ampere's law, where

$$\nabla \times \mathbf{B} = \mu \mathbf{J} \quad (2.9)$$

or using equation (2.3), results in

$$\nabla \times \mathbf{H} = \mathbf{J} \quad (2.10)$$

The boundary conditions for the normal component of \mathbf{B} and tangential components of \mathbf{H} are

$$\mathbf{B}_1 \cdot \hat{\mathbf{n}} = \mathbf{B}_2 \cdot \hat{\mathbf{n}} \quad (2.11)$$

$$\hat{\mathbf{n}} \times (\mathbf{H}_1 - \mathbf{H}_2) = \mathbf{K} \quad (2.12)$$

where \mathbf{K} and $\hat{\mathbf{n}}$ represent the surface current density and the unit vector normal to the surface, respectively.

Figure 2.1, illustrates the boundary surface between two mediums with magnetic permeabilities of μ_1 and μ_2 . The first boundary is defined by shrinking the height of the blue volume and then integrating over the surface area A . According to Gauss's law, the flux around an enclosed area is zero and thus $B_1 = B_2$. In the second boundary condition, the integration is established over a loop (yellow circuit). This definition also follows the logic used above, where the shrinking of the horizontal dimension into a line is accomplished. Lastly, using the Ampere's law, it is possible to show that the tangential component of \mathbf{H} is equal to the surface current density \mathbf{K} .

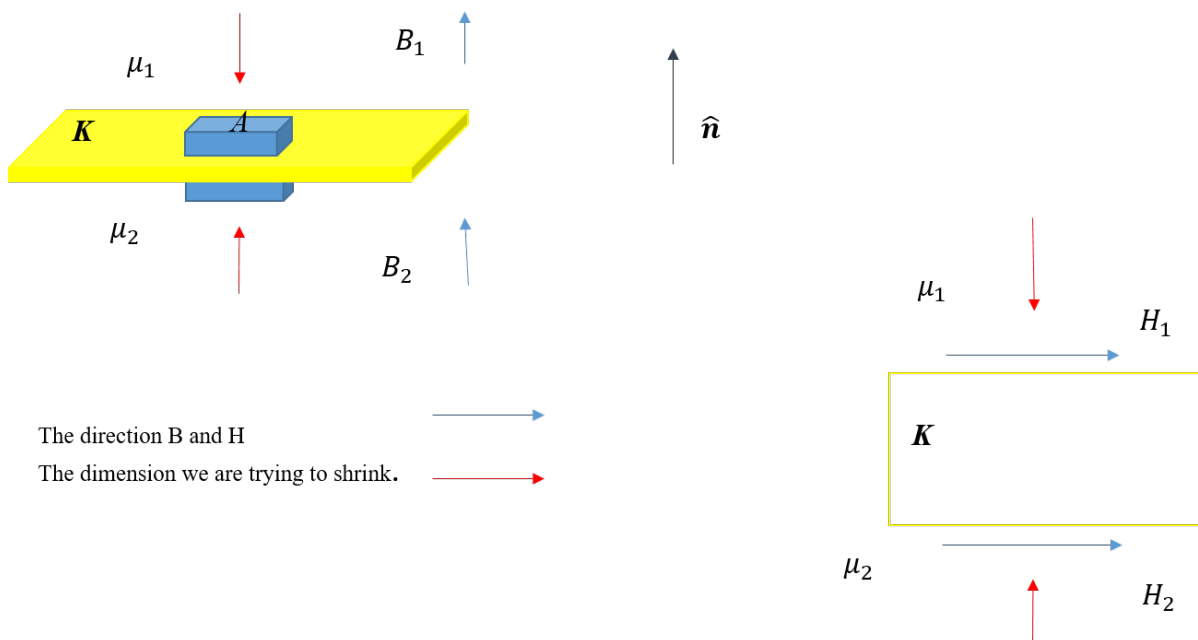


Figure 2.1: Sketch of how the boundary conditions are defined. The first figure in top left depicts the normal boundary of the \mathbf{B} whereas the second one demonstrates the tangential boundary of \mathbf{H} .

One of the solution to the boundaries involves the definition of the fields by the magnetization \mathbf{M} of a material. With the help of some serious amount of vector calculus (*reader could be referred to [7]*), it is possible to derive the Helmholtz theorem for a homogeneous medium and end up with the relations below.

For scalar potential ϕ_p

$$\phi_p(\mathbf{x}) = -\frac{1}{4\pi} \int_V \frac{\nabla' \cdot \mathbf{M}(\mathbf{x}')}{|\mathbf{x} - \mathbf{x}'|} dV' + \frac{1}{4\pi} \oint_S \frac{\mathbf{M}(\mathbf{x}')}{|\mathbf{x} - \mathbf{x}'|} \cdot d\mathbf{S}' \quad (2.13)$$

or alternatively, if we choose the vector potential \mathbf{A}

$$\mathbf{A}(\mathbf{x}) = -\frac{1}{4\pi} \int_V \frac{\nabla' \times \mathbf{M}(\mathbf{x}')}{|\mathbf{x} - \mathbf{x}'|} dV' + \frac{1}{4\pi} \oint_S \frac{\mathbf{M}(\mathbf{x}')}{|\mathbf{x} - \mathbf{x}'|} \times d\mathbf{S}', \quad (2.14)$$

where $\mathbf{x} - \mathbf{x}'$ represents the distance between the source (primed coordinates) and the observation point (unprimed coordinates). The integration is established over a volume V bounded by surface S that contains the observation point. On the other hand the magnetization is assumed to be finite, within a volume V' and surface S' . The solutions to the boundary problems require quite complicated formulations, unless we are dealing with simple geometry. One of the few cases that can be described by analytic closed form solutions is the uniformly magnetized homogeneous ellipsoid, inside a uniform external magnetic field [5].

2.1. INDUCED MAGNETIZATION

When a body finds itself in the vicinity of an external field \mathbf{H} , it can create a magnetic field on its own, due to its atomic structure. Inside the material the microscopic electric currents are described as elementary magnetic moments. The amount of moments aligned with the external field per unit volume accounts for the magnetization \mathbf{M} of the body. The relationship between the applied magnetic field intensity \mathbf{H} and magnetization is defined by

$$\mathbf{M} = \chi \mathbf{H} \quad (2.15)$$

where χ represents the volume magnetic susceptibility of the feature. Depending on χ the material can be mainly be characterized as diamagnetic ($\chi < 0$), paramagnetic ($\chi > 0$) and ferromagnetic ($\chi \gg 0$) (*For more information about the types of magnetic susceptibility the reader may refer to [8]*).

2.2. DEMAGNETIZING FIELDS

The material inside UXOs is typically made by various types of metal, although plastic or composite elements can be used as well. Oxidation is an important factor that impacts the chemical composition of the metal and consequently, its magnetic properties. Nevertheless, UXOs are treated as ferromagnetic objects with solid inner structure ([9]). The assumption above is essential on how we will approach the physics of the magnetic fields.

Figure 2.2 illustrates an example of a ferromagnet. This type of material is characterized by a strong ordering of magnetic moments, even in the absence of an external magnetic field. Moments that have mutual directions are divided into groups, that are called domains and they separated by the domain walls. Note that different directions in the domains (*fig. 2.2a*) may cause the net magnetization to be zero.

In the presence of an external magnetic field, the domains will tend to follow its direction. If the domain motion can be achieved in small field strengths, then the object is characterized as a soft ferromagnet. On the other hand, if the magnetization can occur only in strong fields then the object is refer to as a hard ferromagnet.

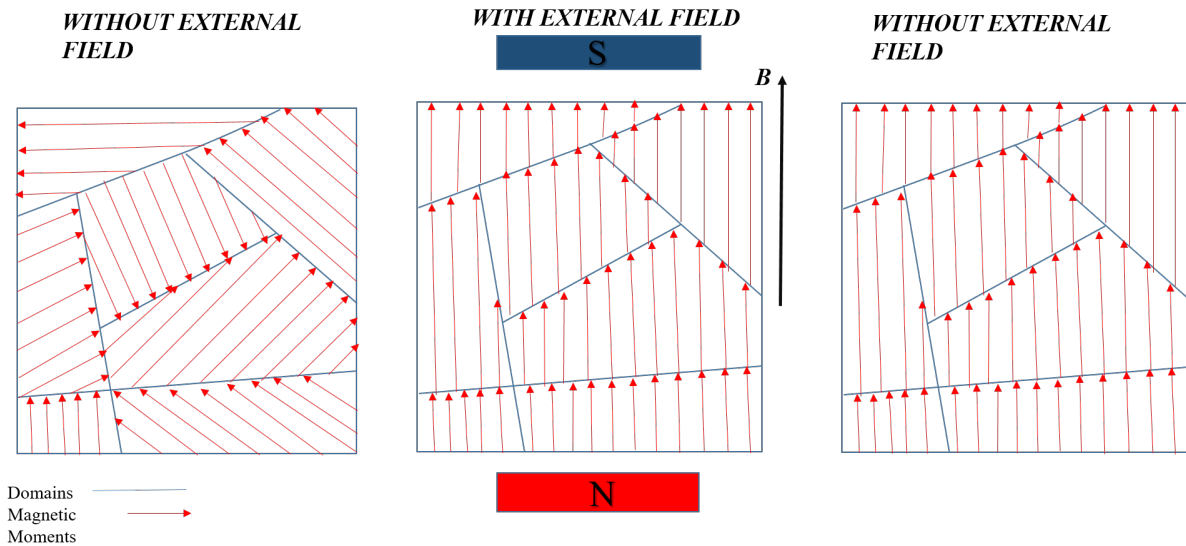


Figure 2.2: Illustration of a ferromagnetic material before, during and after the application of an external field. The magnetic moments will align with the external field and the alignment will remain, even after the field stops occurring.

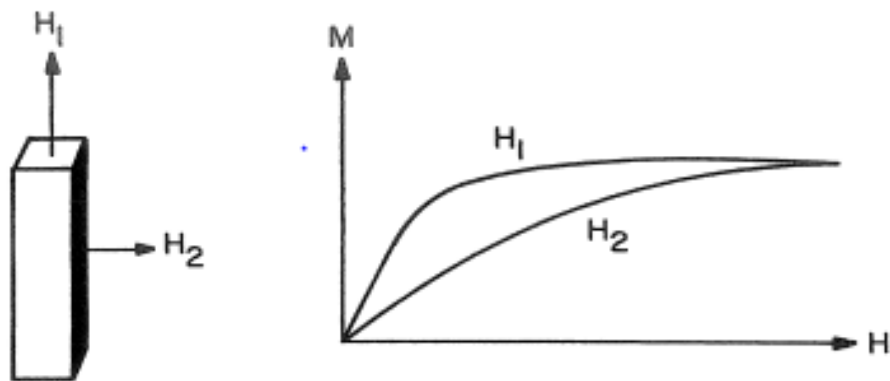


Figure 2.3: Plot showing how the saturation of the magnetization is achieved for magnetizing field along a) the major and b) the minor axis. [10]

Another factor that contributes substantially in the induced magnetization, concerns the shape of the body. Figure 2.3 depicts an example of applying a field in different directions.

Magnetizing an elongated material along the minor axis, requires stronger magnetic field, in order to reach the same amount of magnetization as the long axis. Figure 2.4 depicts a ferromagnetic rectangular shape in the presence of an external field. The magnetization exhibits the same direction as the external field. The materials have finite dimensions, through which the field lines emerge with a normal component. As a result, free poles will be created at the end of each side and a new magnetic field will emanate from the north pole and terminate at the south pole. This field that flows through the sample and acts opposite to the magnetization, is known as demagnetizing field. In the second case, the area of the pole is larger and the distance between the two ends is shorter. Thus, the demagnetizing field is stronger. Generally, the modeling of the demagnetizing fields is rather challenging, since the strength and direction varies inside the material. Only in the case of an ellipsoid they can be considered constant.

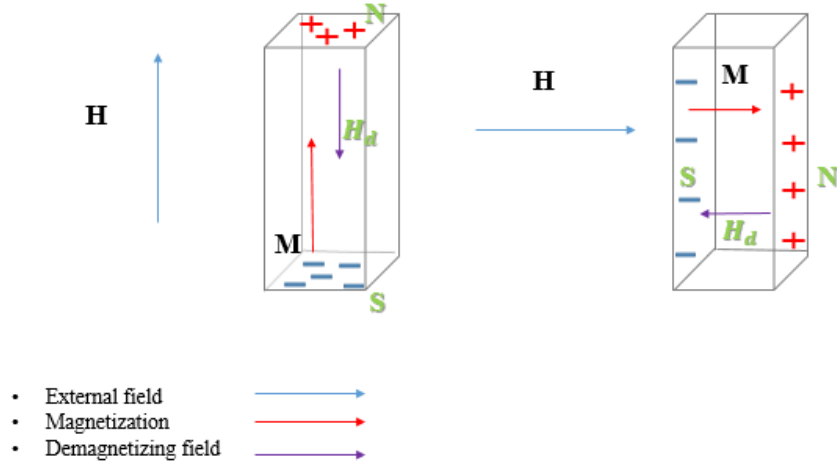


Figure 2.4: Illustration on how the demagnetizing field is created and its direction with respect to magnetization.

2.3. MULTIPOLE EXPANSION

The scalar potential of a uniform magnetized spheroid is described by relationship (2.13). This spheroid is defined by coordinates x_1', x_2', x_3' . Since it is assumed that the magnetization is uniform throughout the body

$$\nabla \cdot \mathbf{M} = 0 \quad (2.16)$$

and (2.13) evolves into

$$\phi_p(\mathbf{x}) = \frac{1}{4\pi} \int_S \frac{\mathbf{M}(\mathbf{x}')}{|\mathbf{x} - \mathbf{x}'|} \cdot d\mathbf{S}' \quad (2.17)$$

thus the scalar potential only relies on the surface integral, namely geometrical shape of the body. The next step concerns the Taylor expansion of $\frac{1}{|\mathbf{x} - \mathbf{x}'|}$ (note that \mathbf{x}' is an arbitrary point inside the source, not the center), about the origin. If $\mathbf{r} = |\mathbf{x} - \mathbf{x}_o'|$ then $r = \|\mathbf{r}\|$ is the euclidean distance between the observation point and the center of the source. Since the magnetization occurs only inside the body, there is no need to keep mentioning that is function of the source. Thus, we are dropping the (\mathbf{x}') .

$$\begin{aligned} \phi_p(\mathbf{x}) = & \frac{1}{4\pi r} \int_S \mathbf{M} \cdot d\mathbf{S}' + \frac{\partial}{\partial x_i'} \frac{1}{4\pi r} \int_S x_i' \mathbf{M} \cdot d\mathbf{S}' + \\ & \frac{\partial^2}{\partial x_i' \partial x_j'} \frac{1}{4\pi r} \frac{1}{2!} \int_S x_i' x_j' \mathbf{M} \cdot d\mathbf{S}' + \\ & \frac{\partial^3}{\partial x_i' \partial x_j' \partial x_k'} \frac{1}{4\pi r} \frac{1}{3!} \int_S x_i' x_j' x_k' \mathbf{M} \cdot d\mathbf{S}' \dots \end{aligned} \quad (2.18)$$

The repeated indices denote that a summation sequence has to be used. The scalar potential of 2^n pole that also has magnetic moment of $m_{i,j,\dots}^n$ is obtained by the expression

$$\phi_p(\mathbf{x})^{2n} = \frac{m_{i,j,\dots}^n}{4\pi n!} \frac{\partial^n}{\partial x_i' \partial x_j' \dots} \frac{1}{r} \quad (2.19)$$

and thus

$$m^{(0)} = \int_S \mathbf{M} \cdot d\mathbf{S}' \quad (2.20)$$

$$m_i^{(1)} = \int_S x_i' \mathbf{M} \cdot d\mathbf{S}' \quad (2.21)$$

$$m_{ij}^{(2)} = \int_S x_i' x_j' \mathbf{M} \cdot d\mathbf{S}' \quad (2.22)$$

$$m_{ijk}^{(3)} = \int_S x_i' x_j' x_k' \mathbf{M} \cdot d\mathbf{S}' \quad (2.23)$$

The equation (2.20) describes the magnetic moment of scalar monopole. As mentioned before, monopoles do not exist and therefore (2.20) is zero. Equation (2.21) is referred to the dipole moment term. This term is the dominant one, even if the scope of the survey, exceeds the dimensions of the object. The relation (2.22) is attributed to the quadrupole, but because of the symmetry of the body, this term is zero as well. Finally, (2.23) defines the octupole term, that is usually omitted when the measurements are assumed to be at significant distance from the body.

Example of how the evaluation of the integrals is accomplished will be given in (2.25). For dipole integral evaluation we are not going to assume that the magnetization is constant throughout the body. Instead:

$$m_i^{(1)} = \int_S x_i' \mathbf{M} \cdot d\mathbf{S}' - \int_V \nabla' \cdot \mathbf{M} dV'. \quad (2.24)$$

Using the integration by parts identity, we end up with

$$m_i^{(1)} = \int_V \mathbf{M} \cdot \nabla' x_i' dV' = \int_V M_i dV', \quad (2.25)$$

or

$$\mathbf{m} = V' \mathbf{M} \quad (2.26)$$

which means the dipole moment represents the integration of the magnetization along the volume of the object [11]. For the quadrupole, the magnetization is uniform throughout the body and there is symmetry along the major axis of the spheroid. Like the monopole, the quadrupole is also zero. Analysing the integrals for the octupole is quite challenging. The magnetic moment is described by 3×3 tensor, with 27 elements. Investigating (2.23), as well as assuming that there is axial symmetry, the number of independent parameters is reduced to 6. These are:

$$\begin{aligned} m_{111}^{(3)} &= 3m_{221}^{(3)} = 3M_1 I_{11} \\ m_{222}^{(3)} &= 3m_{112}^{(3)} = 3M_2 I_{11} \\ m_{222}^{(3)} &= 3M_3 I_{33} \\ m_{113}^{(3)} &= m_{223}^{(3)} = M_3 I_{11} \\ m_{331}^{(3)} &= M_1 I_{33} \\ m_{332}^{(3)} &= M_2 I_{33}. \end{aligned} \quad (2.27)$$

If these parameters are known, then it is possible to infer the rest of them by,

$$\begin{aligned} m_{ij}^{(3)} &= m_{ji}^{(3)} = m_{jii}^{(3)} \\ m_{i,j,k}^{(3)} &= 0, \text{ when} \\ & i \neq j \neq k. \end{aligned} \quad (2.28)$$

2.3.1. MODELLING AN ELLIPSOID

If it is inferred that the object in question is a spheroid with length L , diameter α and aspect ratio e ($e = \frac{\alpha}{L}$), then I_{11} and I_{33} are described by

$$\begin{aligned} I_{11} &= \frac{4\pi}{15} e \alpha^5 \\ I_{33} &= \frac{4\pi}{15} e^3 \alpha^5. \end{aligned} \quad (2.29)$$

The last step concerns the acquisition of the magnetization vector. In the presence of an external field, or in this case the Geomagnetic Field \mathbf{b}_o , the magnetization is given by (2.30)

$$M_i = \mu_o^{-1} F_i b_{oi}, \quad (2.30)$$

where $i=1,2,3$. The calculation of the demagnetization factors F_i is given by the expression (2.31), where the magnetic permeability of the spheroid is $\mu_{r1}\mu_o$ and whereas permeability of the background material is $\mu_{r2}\mu_o$.

$$F_i = \frac{\mu_{r1} - 1}{1 + \frac{\Xi_i(\mu_{r1} - \mu_{r2})}{2\mu_{r2}}} \quad (2.31)$$

For the magnetic survey to be successful, there has to be a contrast between the magnetic properties of the object and the background material. This is usually the case though in some places, concentrations of the magnetic material may cause interference with the detection of UXO [12]. Nevertheless, the calculation of the demagnetization factors, is rather insensitive to μ_{r1} and μ_{r2} . Thus, it is possible to use fixed values for $\mu_{r1}=500$ and $\mu_{r2}=1$ without including too much of uncertainty. The Ξ_i s are factors that depend on the shape of the body and are specified by the relations (2.32) and (2.33).

There are three demagnetization factors that are attributed to the three principal axis of the ellipsoid. In general, $F_1 + F_2 + F_3 = 1$. In case the model in question is a sphere, where all the axes are the same, then the these factors are equal to $\frac{1}{3}$. In the case of ellipsoid, the derivation of these factors is quite challenging. Usually, it is preferred to use the ellipsoid of revolution, where two of the principal axes have equal length. Thus,

$$\Xi_1 = \Xi_2 = \frac{e(e+E)}{e^2-1} \quad (2.32)$$

$$\Xi_3 = \frac{-2e(e^{-1}+E)}{e^2-1} \quad (2.33)$$

For a prolate spheroid $e > 1$:

$$E = \frac{\arctan \frac{e}{\sqrt{1-e^2}} - \frac{\pi}{2}}{\sqrt{1-e^2}} \quad (2.34)$$

For an oblate spheroid $e < 1$:

$$E = \frac{\log e - \sqrt{e^2-1}}{\sqrt{e^2-1}} \quad (2.35)$$

For a sphere, $e=1$ so the $\Xi_1 = \Xi_2 = \Xi_3 = \frac{2}{3}$ [5].

The relation of the field induced by the spheroid and includes terms up to the octupole is given by relations 2.36

$$\mathbf{b}_s = \mathbf{b}_s^{(1)} + \mathbf{b}_s^{(2)} + \mathbf{b}_s^{(3)} \quad (2.36)$$

where

$$b_{si}^{(1)} = \frac{\mu_o}{4\pi r^3} \left(\frac{3}{r^2} [\mathbf{r} \cdot \mathbf{m}^{(1)}] r_i - m_i \right) \quad (2.37)$$

is the dipole field,

$$b_{si}^{(2)} = \frac{3\mu_o}{8\pi r^5} \left(-r_i m_{jj}^{(2)} - r_j (m_{ij}^{(2)} + m_{ji}^{(2)}) + 5r^{-2} r_i r_j r_k m_{jk}^{(2)} \right) \quad (2.38)$$

is the quadrupole field (*though it is zero in our case*) and

$$b_{si}^{(3)} = \frac{\mu_o}{8\pi r^5} \left(3m_{ijj}^{(3)} - 15r^{-2} [r_i r_j m_{jkk}^{(3)} + r_j r_k m_{ijk}^{(3)}] + 35r^{-4} r_i r_j r_k r_l m_{jkl}^{(3)} \right) \quad (2.39)$$

is the octupole field.

3

FORMULATION OF THE PROBLEM

Billings et al. 2002 provided a specific procedure on how to deal with UXO modelling and discrimination. The first step concerned the estimation of the magnitude and the position of the magnetic moment, while the next step used the acquired magnetic moment to identify it.

3.1. INVERSION

During a magnetic survey magnetic measurements are collected. The goal is to try and find a model that can explain the data. This can be achieved by the inversion process where one can use a model to produce data that will approximate the measurements. In other words the aim is to achieve the minimum difference between the measured and the calculated data. It is important to note that the measurements contain noise and therefore the difference could never be zero.

3.2. INVERSION METHOD

First in order to decide the inversion method, it is important to consider the amount of knowns and unknowns. There are two types of magnetic measurements:

The first one considers total field anomaly measurements. From the previous chapters it is concluded that both the geomagnetic field \mathbf{b}_o as well as the field due to a magnetic spheroid \mathbf{b}_s , contribute to the total field measurements \mathbf{b}_{tot} at a location \mathbf{x} . In addition, the magnetic anomaly \mathbf{b}_a is defined by $\mathbf{b}_a = \|\mathbf{b}_{tot}\| - \|\mathbf{b}_o\|$. There are two assumption here. The first one considers only the dipole field, since fields of higher orders are rapidly decaying and the second one assumes that the dipole field is way smaller than the geomagnetic one (*The specifics about the derivation of (3.1) and (3.2) can be found at [13]*). Thus,

$$\mathbf{b}_a = \mathbf{b}_s \cdot \hat{\mathbf{b}}_o \quad (3.1)$$

or

$$\mathbf{b}_a = \frac{\mu_o}{4\pi} \left[\frac{3(\mathbf{m} \cdot \mathbf{r})\mathbf{r} \cdot \hat{\mathbf{b}}_o}{r^5} - \frac{\mathbf{m} \cdot \hat{\mathbf{b}}_o}{r^3} \right] \quad (3.2)$$

where

$r = [x, y, z]^T$ is the distance between the source and the observation point in the 3 dimensional space while $\hat{\mathbf{b}}_o = [\hat{\mathbf{b}}_{ox}, \hat{\mathbf{b}}_{oy}, \hat{\mathbf{b}}_{oz}]^T$ contains the directions of the geomagnetic field [13]. The coordinate system that is used for the Earth's magnetic field is the one provided by the IGRF [International Geomagnetic Reference Field] where the x is positive towards the North, y is positive towards the East and z is positive downwards.

2) Gradient magnetic measurements

$$\mathbf{b}_{a_z} = \frac{\mathbf{b}_{a_lower} - \mathbf{b}_{a_upper}}{dz}, \quad (3.3)$$

where the \mathbf{b}_{a_z} describes the vertical component of the anomaly, \mathbf{b}_{a_lower} and \mathbf{b}_{a_upper} are the total anomaly field fields detected on the lower and upper sensor respectively. The denominator defines the vertical distance between them.

In addition, \mathbf{m} is given by

$$\mathbf{m} = V'\mathbf{M} \quad (3.4)$$

where

$$V' = \frac{\pi}{6}ea^3 \quad (3.5)$$

and

$$\mathbf{M} = \mu_o^{-1}\mathbf{R}^T\mathbf{F}\mathbf{R}\mathbf{b}_o \quad (3.6)$$

The magnetization of a spheroid is described by equation (3.6) which contains the demagnetization factors. It is important to consider that not only the shape of the spheroid impacts the induced magnetic field, but also the orientation of the body with respect to the Earth's magnetic field. In the case of sphere, where the three aspect ratios are equal and the remanent magnetization is negligible, the dipole direction is assumed to be aligned with the direction of \mathbf{b}_o . On the other hand, if the object in question has ellipsoidal shape, the orientation of the body is also an important parameter that needs to be taken into account. The latter is accomplished by introducing the Euler angles. Figure 3.1 demonstrates the corresponding coordinate system. The induced magnetic field is assumed to have the direction of the major axis. The angles θ and ϕ correspond to the rotation angles along the East and North, respectively. Due to the symmetry of the spheroid the third angle is zero. The way to insert the angles in the equation (2.30) is by including the Euler rotation matrix that will rotate the \mathbf{b}_o to spheroid centered coordinates and then the transverse \mathbf{R}^T will rotate the magnetization back to the space centered ones.

A derivation of the \mathbf{R} matrix, as well as an explanation regarding the rotations will be given in the next chapters.

Considering the above, the modeling of the magnetic anomaly requires seven unknown parameters $(x,y,z,\theta,\phi,\alpha,e)$, where x,y,z are the coordinates of the body, θ and ϕ are the rotation angles, α is the spheroid diameter (or the length of the minor axis) and e is the aspect ratio. Thus, the system is under-determined with only known parameter being the magnetic measurements and therefore a non-linear solver needs to be constructed.

3.2.1. BUILDING THE CODE

The conventional way of dealing with inverse problems is to specify an objective function $f(\mathbf{m})$ with \mathbf{m} being the seven model parameters and then try to minimize that particular function, as much as possible. (Note that this symbol is different from the one we use to refer to the magnetic moment \mathbf{m}). In this case, the chosen objective function is the root-mean-square-error (3.7) between the predicted and the the observed values[14].

$$RMSD = \sqrt{\frac{\sum_{i=1}^n (d_{mod}(\mathbf{m}) - d_{obs})^2}{n}} \quad (3.7)$$

The $d_{mod}(\mathbf{m})$ represents the data that were calculated using the equations in section 3.4.1, d_{obs} is referred to the observed data and n is the number of data used in the inversion.

It is mentioned above that the aim is to minimize the function. A way of approaching this problem is to differentiate this function with respect to the model parameters and then try to locate the minimum value. This thought of process will invoke the first order iterative optimization algorithms. There are several gradient methods that can solve problems iteratively, such as the steepest descent, the Gauss-Newton, the conjugate gradient, each one them is defined by their own difficulties and flexibilities.

This thesis uses the first one, since it is quite simple and allows the user to manipulate the step size in order to control the convergence. Specifically the code will start with an initial guess \mathbf{m}_n . Let's also assume that the updated model is \mathbf{m}_{n+1} and the step length is β . Then

$$\mathbf{m}_{n+1} = \mathbf{m}_n - \beta \nabla f(\mathbf{m}_n) \quad (3.8)$$

Equation (3.8) will update the model with proper modifications in the parameters that are controlled by the β , until the requested precision is achieved. More discussion about determination of β will be provided in the next chapter.

It is important to note that gradient algorithms help solving initial value problems, namely problems that are highly reliant on the initial guess. If the starting model is not close to the actual values, then it is possible to get stranded at a local minimum. That of course, is also a function of the step length. If the value is too small, then the possibility of getting trapped is high, whereas if it is too large, then the inversion can become unstable.

Lastly, the gradients were approximated with the help of the central finite difference method. If we assume that n_i is a point of the function $f(\mathbf{m}_i)$ with respect to i parameter, then the gradient will be considered the difference between the previous n_{i-1} and the next n_{i+1} values of a that particular point, dividing it by their distance h_i .

$$\frac{\partial f(\mathbf{m}_i)}{\partial \mathbf{m}_i} = \frac{f(\mathbf{m}_i + h_i) - f(\mathbf{m}_i - h_i)}{2h_i}. \quad (3.9)$$

In order to approximate the gradient, the distance between the two points has to be minimum. On the other hand, very small choices for h can increase computational time. By performing tests to each one of the parameters, it was established that the appropriate h was 0.01 for all them. Smaller h had a negligible impact on the values of the gradients.

3.3. SYNTHETIC RESULTS

Before incorporating real data into our study, it is essential to analyze the code a bit further, in order to establish an expected behavior. Example of this be could related to how the model behaves when the Euler angles are varied, or how well can an acceptable model can be recovered, even if its initial values, diverge from the real ones.

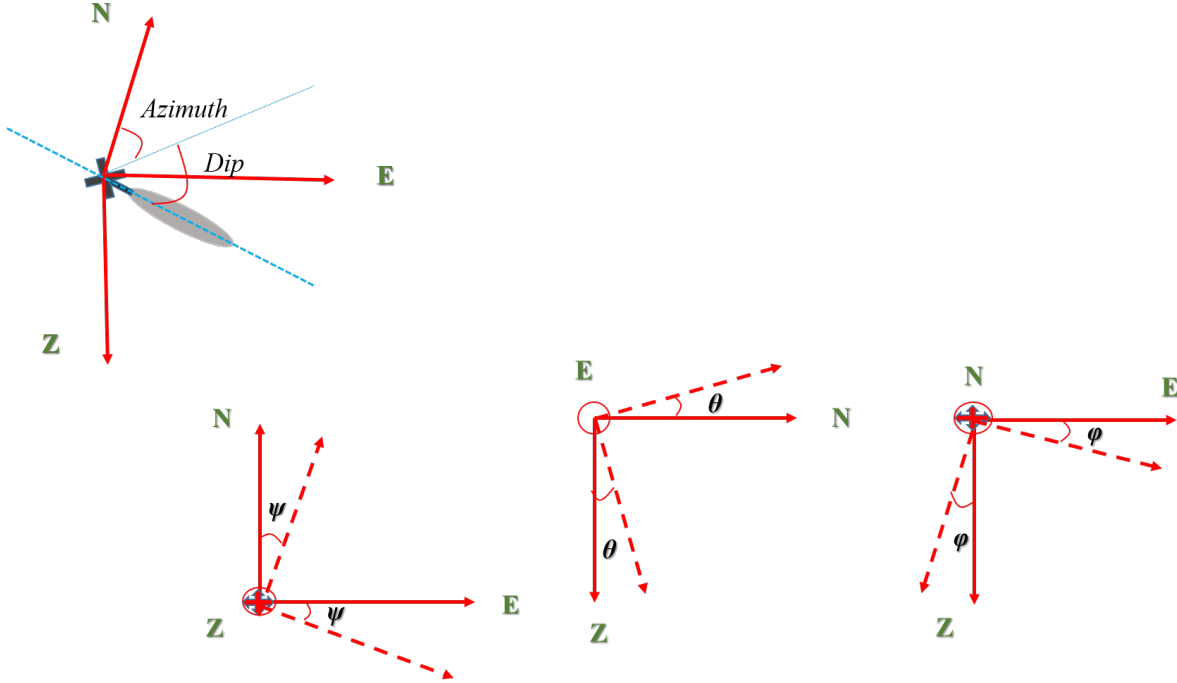


Figure 3.1: Rotation angles. The sketch in the upper left corner depicts the spheroid centered coordinate system. The North, East and Down system is given in spherical coordinates. The second sketch the lower left corner illustrates a rotation along the Z axis, the one in the middle along the East axis and the right one along the North axis. Those angles might be different from the dip and azimuth angles.

Figure 3.1 explains how rotation angles work. First of all, a coordinate system needs to be established. In this case it is assumed that \mathbf{X} is positive to the North, \mathbf{Y} is positive to the East and \mathbf{Z} is positive downwards. The magnetization in eq. 3.6 requires the geomagnetic field to be solved in spheroid centered coordinates, so it will coincide with the major axis of the object.

As mentioned above, there are three Euler angles. The angle ψ , θ and ϕ denote the angles where the body is rotated along the Z, East or North axis respectively. Their corresponding rotation matrices for each case are:

$$\mathbf{Z} = \begin{bmatrix} \cos \psi & \sin \psi & 0 \\ -\sin \psi & \cos \psi & 0 \\ 0 & 0 & 1 \end{bmatrix} \quad (3.10)$$

$$\mathbf{Y} = \begin{bmatrix} \cos \theta & 0 & -\sin \theta \\ 0 & 1 & 0 \\ \sin \theta & 0 & \cos \theta \end{bmatrix} \quad (3.11)$$

$$\mathbf{X} = \begin{bmatrix} 1 & 0 & 0 \\ 0 & \cos \phi & \sin \phi \\ 0 & -\sin \phi & \cos \phi \end{bmatrix} \quad (3.12)$$

A rotation sequence first about the X axis, then about the Y axis and lastly about the Z axis will result to a directional cosine matrix that has the form of:

$$\mathbf{R} = \begin{bmatrix} \cos \theta \cos \psi & \cos \theta \sin \psi & -\sin \theta \\ \cos \psi \sin \theta \sin \phi - \cos \phi \sin \psi & \cos \phi \cos \psi + \sin \theta \sin \psi \sin \phi & \cos \theta \sin \phi \\ \cos \phi \cos \psi \sin \theta + \sin \phi \sin \psi & -\cos \psi \sin \phi + \cos \phi \sin \theta \sin \psi & \cos \theta \cos \phi \end{bmatrix} \quad (3.13)$$

Examples of how the rotations work, are given in the figures 3.2. The ellipsoidal body of 10cm diameter and aspect ratio of 4, is placed at the depth of 70cm. The location is considered at the North pole, where the inclination and declination of geomagnetic field is 90 and 0 degrees respectively. It is important to acknowledged that only the X and Y rotations are important, while the rotation along the Z axis is neglected due to the spheroid's symmetry. Instance A, depicts a case where both angles are zero. For the examples B and C, the rotation along the X axis is zero, while the corresponding θ s are 90 and -90 degrees. Lastly D, E and F, represent cases where the rotations are described by $\phi, \theta = 45, -45$, $\phi, \theta = 45$ and $\phi, \theta = -45$. Finally, looking at the colorbar, one can deduce some information on how the strength of the anomaly varies as the orientation and declination of the object changes. The anomalies caused by object with inclinations are stronger than the corresponding ones from horizontal orientations.

From the next chapters, ϕ and θ will be the rotation angles. The angle from the North is going to be referred as azimuth, while the angle from the horizontal will be called dip.

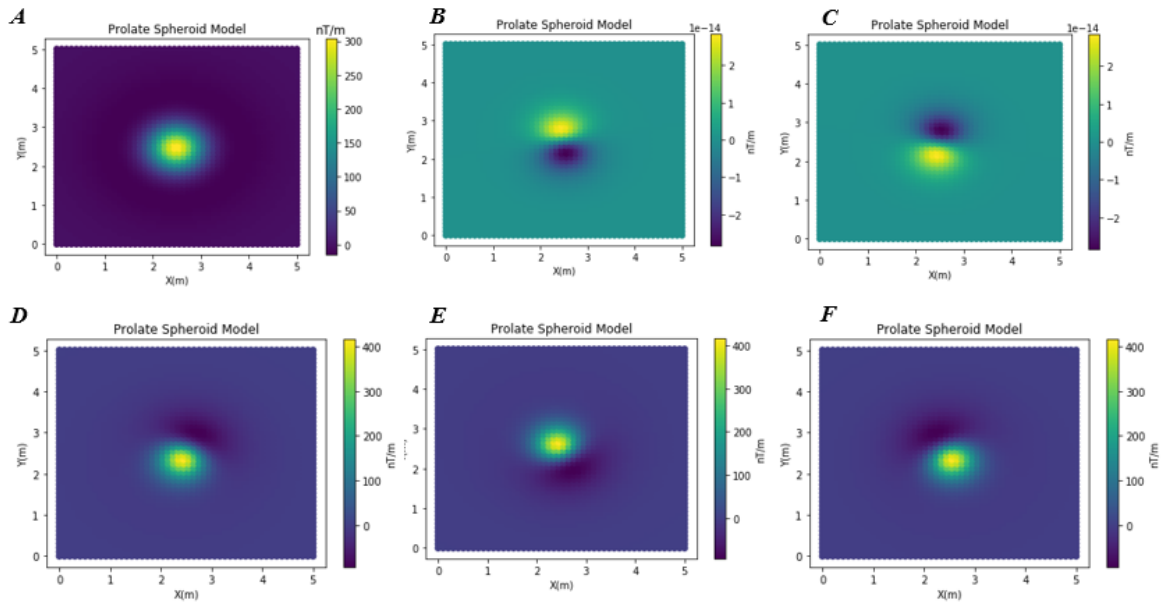


Figure 3.2: Results for different angles. The object is placed in the North Pole where the inclination is 90° . A) The rotation angles are zeros, therefore the dipole is vertical, in the direction of the field. B) $\phi=0$ and $\theta = 90^\circ$. The dipole is found in horizontal position, with an azimuth of 0° . C) Same as B, though the azimuth is 180° . D) $\phi = 45^\circ$ and $\theta = -45^\circ$. The dipole has a dip of 45° and an azimuth of 45° from the North. E) $\phi = 45^\circ$ and $\theta = 45^\circ$. Same dip as D, but its direction is 135° from the North. F) $\phi = -45^\circ$ and $\theta = -45^\circ$. Same as dip angle as the last two, with an azimuth of 315° .

The following step involves a rough evaluation of the accuracy of the results. Handling seven unknown parameters requires a lot of caution, due to the fact that small changes in one parameter can result in major changes in another. Equivalently, important changes in one parameter, may be hidden by the larger changes in the others. A way to tackle this problem is to scale the gradients, namely scale the amount of variation each model parameter is allowed to have, in each iteration. For example, the object that was mentioned above will be placed in the middle of a 5×5 area and depth of one meter. Both angles are 45 degrees (table 3.1). Gaussian noise was also added to imitate a real situation. Figure 3.3

illustrates the situation where all the parameter are the same, except the depth. No scaling was added to the parameters. In order for all the parameters to be stable the amount of change or the beta had to be extremely small and the performance of the inversion in general was quite poor. On the other hand, if the scaling is appropriate, the results are pretty close to the real ones. Ideal scaling is when the changes in other parameters are kept to minimum, while the depth is free to vary. Models with half a meter and one meter differences are depicted in figures 3.3. Both achieved reasonable results, though the latter required more iterations. More tests were conducted, in which the other parameters were allowed to vary. The results are demonstrated in Appendix A. With the right scaling, all the inversions were able reach close the real situation.

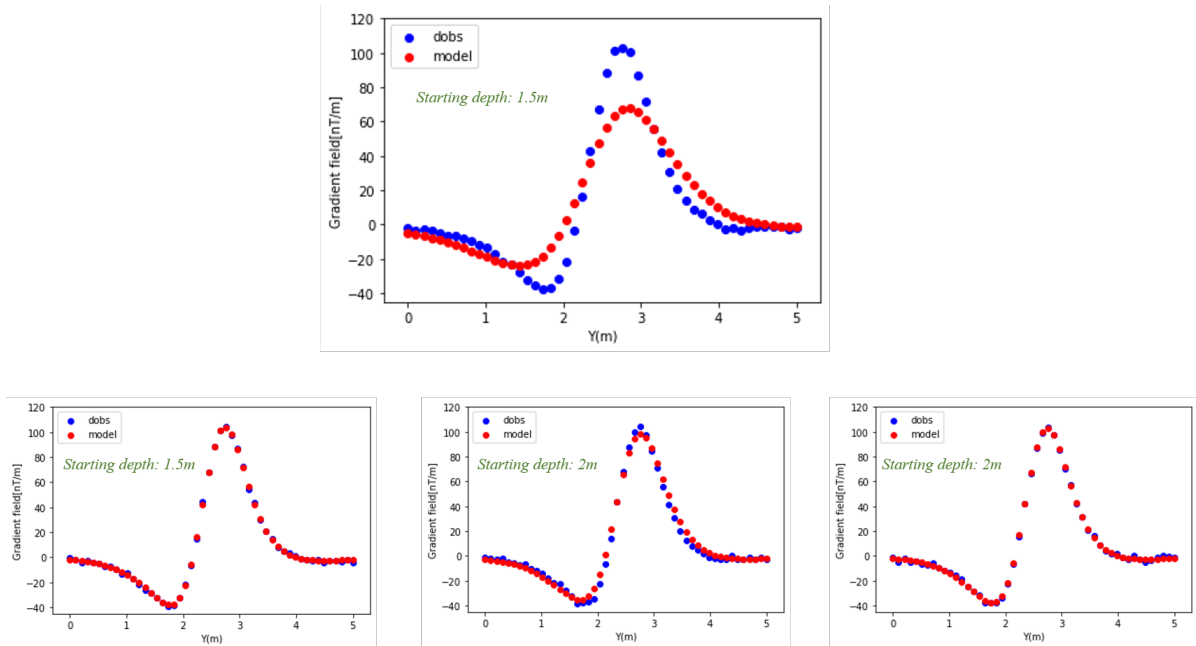


Figure 3.3: Multiple test with a varying depth. The figure at the top, illustrates a non-scaled inversion. The one at the bottom left has a starting depth that deviates half a meter from the observed one, while the other two have a starting depth of 2 meters. Their difference lies in the number of iterations.(A,B,C,D required 100,95,100 and 200 iteration respectively).

	Position (m)	$\phi, \theta(^{\circ})$	α (m)	ϵ (-)
"Real" model	x=2.5 y=2.5 z=1	45, 45	0.1	4
Initial Model 1	x=2.5 y=2.5 z=1.5	45, 45	0.1	4
Initial Model 2	x=2.5 y=2.5 z=2	45, 45	0.1	4

Table 3.1: Table containing the parameters with initial values used in inversions presented in 3.3.

4

REAL RESULTS

The next step involved the evaluation of the code with measurements of actual UXO.

4.1. RIVER VERIFICATION TRIAL

The first evaluation was against a dataset, collected in december 2020, as a trial survey at the start of an UXO campaign in the southern part of the Netherlands. Prior to the start of the survey, a system verification had been performed where an actual UXO was placed on the riverbed and a number of measurement lines collected over the item, to verify system functionality and positioning accuracy. These data were collected by 10 Sensys FGM3D100 fluxgates in a two-row of five magnetometer configuration. Their separation distance was 1m. Both total field anomaly, as well as gradiometry data were available. In addition, measurements with different heights were accomplished. For the purpose of the thesis we chose to invert gradient data taken at two meters height (*namely the lower sensor had a two-meter distance from the object*) and total field anomaly data at one meter height. The UXO was a 4.2 ich (*approximately 10.7cm*) mortar with length of approximately 30cm. Lines measurements with multiple directions were also performed. The results from the inversion are shown in figures 4.1 and 4.2. Overall, both of them yield satisfactory results, namely they were able to produce a model that resembled the measured object. The gradient data generated better fits than the total field anomaly data, with the one taken in the E-W being the best of all. Note that since all four tests managed to capture the object, a better fitted model qualifies as the one with the least residuals. In both configurations the E-W measurements delivered a somewhat larger values of the body dimension that resulted in a small rise in the magnetic moment. The error of the depth appeared to be between 0.01 and 0.2m, values that are within an acceptable uncertainty, since the survey was performed on a boat and the position was not very accurate. Lastly, the recovered angles showed an almost perpendicular orientation to the geomagnetic field with azimuth around 60° (or 30° from the East).

4.1.1. COMPARISON WITH SPHERE

An algorithm for a sphere model was provided by the League Geophysics team. This code used a linear inversion to recover the magnetic moment and then this magnetic moment was inserted in a non-linear solver to retrieve the position of the dipole. The main equation used in the forward modelling for both the linear and the non-linear inversion, is the same as the one in (3.2). It was also assuming that the volume of the object is 1 m^3 . The magnetic moments as well as the position of the object were quite comparable with difference only in the order of 10^{-2} . On the other hand the fit of the sphere model in general was better (*in terms of smaller residuals*) than the analogous of the spheroid. This could be because the latter considers more parameters that affect the induced field such as the volume, the shape and the orientation of the body. In other words, adding more parameters to the mix, means adding

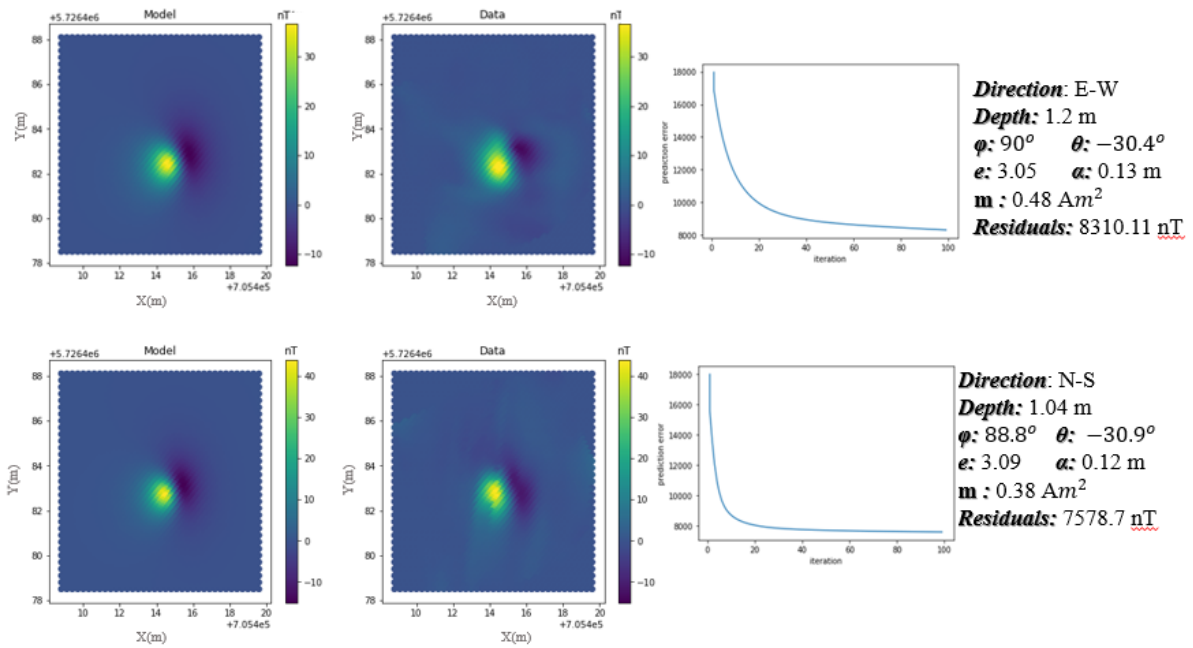


Figure 4.1: Inversion results, for total field anomaly measurements collected at 1 meter.

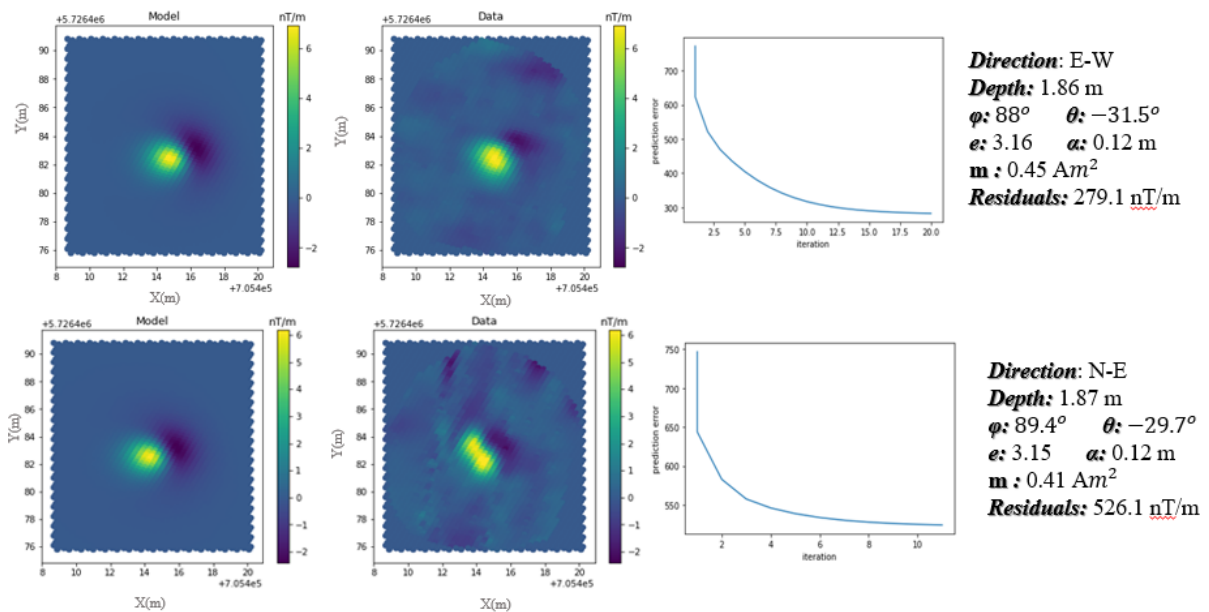


Figure 4.2: Inversion results, for gradient measurements collected at 2 meters height. The difference in the fit is exaggerated by the less amount of data, used to speed up the process in the gradient measurements. Nevertheless the better fit still stands.

more uncertainties. In this regard, the spherical model can be considered superior to the spheroid. Nevertheless, the spheroid was successful enough to recover the magnetic dipole moment, its position and dimensions so a crude identification is possible in this case as well. The square residuals of the total field measurements are displayed in the figures 4.3 and 4.4.

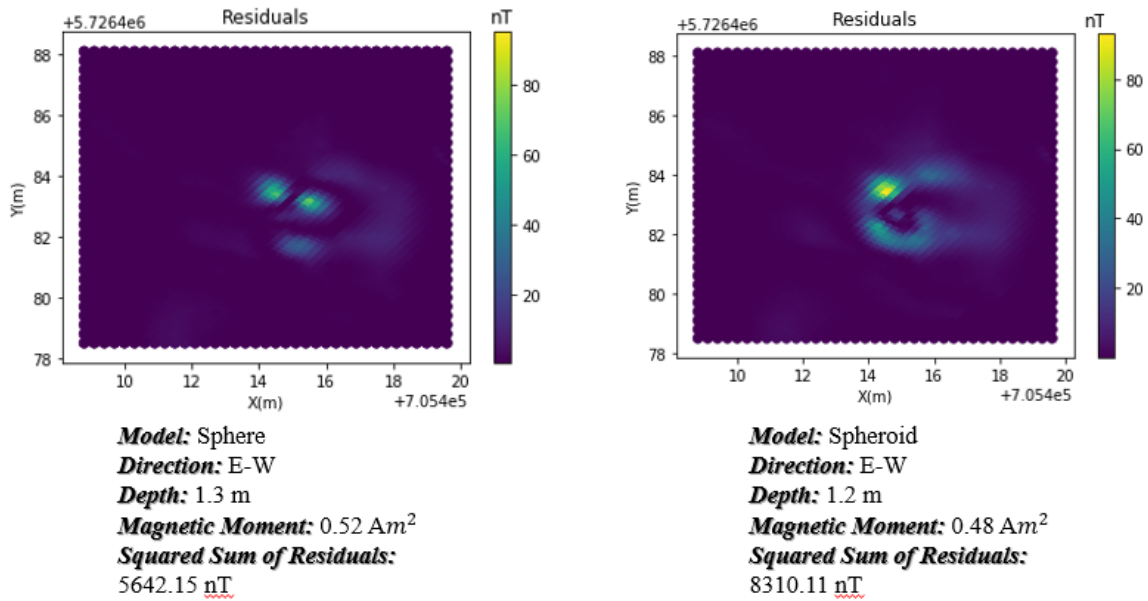


Figure 4.3: Maps of squared residuals between Total Magnetic Field Anomaly measurements and A) the spherical model or B) the spheroid model. The direction of the line is EW.

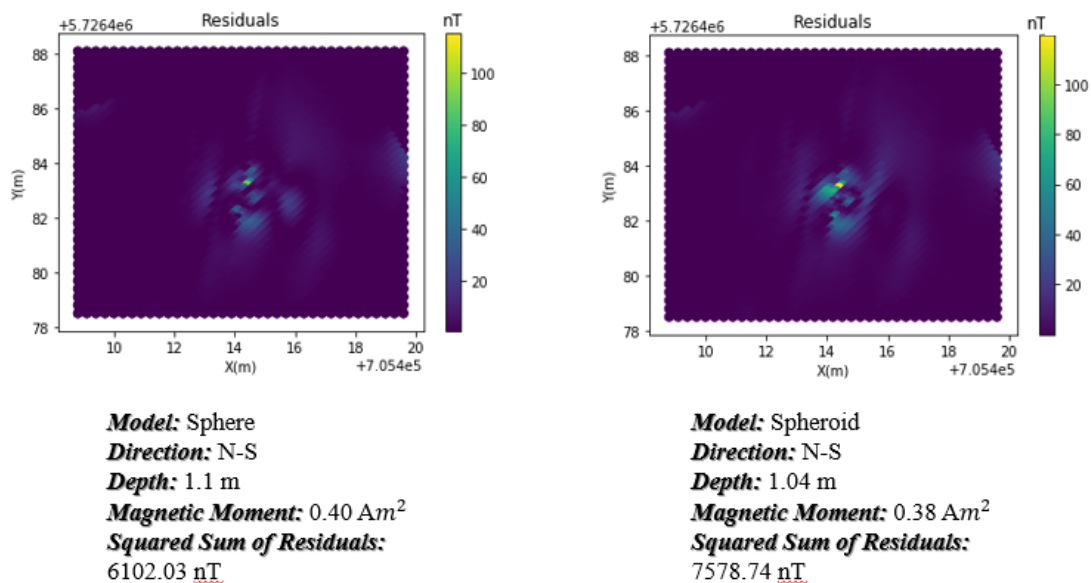


Figure 4.4: Maps of summed residuals between Total Magnetic Field Anomaly measurements and A) the spherical model or B) the spheroid model. The direction of the line is NS.

4.2. REASEURO DATA

Reaseuro is a dutch company specializing in land-based UXO identification and clearance. A one day field trip to the Reaseuro headquarters allowed us to collect information on UXO with a characteristic prolate shape. Four different types of (actual used but defused and rendered inert) amunitions were used:

- 1) A 60mm steel casing hand grenade with 115mm height.
- 2) A 10cm cast iron cannonball from the early 19th century.
- 3) A 3 inch steel (or 76.2mm) WWII casing mortar with 400mm length.
- 4) A WWII steel 25-pound British shell, with diameter and length of 87.6mm and 328mm respectively.

During the acquisition of the magnetic data on the REASEURO testing ground, the angle and the orientation of the body was varied (table 4.1). Afterwards, the collected measurements were pre-processed, corrected for the difference in speed, detrended and inserted into the non-linear inversion code.

4.2.1. UNCERTAINTIES

The next chapters will include a thorough discussion of the inversion results. It is important to consider the sources of uncertainty that can contribute to possible variations from the real situation, but also in differences between the tests themselves. The burial depth is supposed to be set around 0.5 meters, plus the height of the instrument that was around 0.1 meters. There was no GPS installed during the measurements so it is normal to have a uncertainty of ± 0.2 meters in the horizontal as well as the vertical position, due to moving the objects between the tests. In addition, possible uncertainties could rise due to the pre-processing. For example, the lag correction might not be ideal and it might cause smearing of anomaly or the filtering of the background noise, might introduce errors in the main signal.

UXOS	GRENADE	CANNON BALL	MORTAR	BRITISH SHELL
Test 1	Vertical	As a sphere it does not have particular direction	Horizontal and in the direction of geomagnetic field	Horizontal and in the direction of geomagnetic field
Test 2	Horizontal and in the direction of the geomagnetic field	Not changed	Angle of approximately 45 degrees in the direction of the geomagnetic field	Angle of approximately 45 degrees in the direction of the geomagnetic field
Test 3	Horizontal and at angle of 90 degrees w.r.t the geomagnetic field	Placed at angle of 90 degrees w.r.t to its original position	Horizontal and at angle of 90 degrees w.r.t the geomagnetic field	Horizontal and at angle of 90 degrees w.r.t the geomagnetic field

Table 4.1: Information about the orientation of the UXOs, in each test.

4.2.2. HAND GRENADE

Figure 4.5 shows the anomalies from the grenade in three different orientations. It is clear that in this case only the inclination matters and not the angle with the magnetic North. It seems that the aspect ratio is not large enough to affect the direction of the induced magnetization. The recovered x and y positions are fairly similar with the real ones, within the uncertainty range. On the other hand, there is approximately 0.1 m of a difference in depth, between each test. There could be a number of explanation for these deviations, for example due to the reason that was mentioned in 4.2.1 or due

to inadequate scaling. An important thing to remember is that the coordinate system in this case is different from the examples with the synthetic data. The measurements have taken place in Netherlands where the inclination is $I = 68.9^\circ$ and the declination $D = 2^\circ$ and therefore the interpretation of the rotation angles is different that the ones as if the object was located in the North pole. In the cases of test 2 and 3, the body was placed horizontally, though there is a hint of dipping, around 10° towards the North. Their azimuths are approximately 190° from the North (110° from the East). In case 1, where the object is vertical, there is also a very small a inclination, about in the NW direction. That could possibly be a deviation due to a possible movement of the object during the burial or an indication that a certain percentage of remanent magnetization exists that deviates the direction of the induced magnetic field, from the direction of the major axis. The recovered aspect ratios from each test, have a difference of 0.2 while the diameters differ of about 20 millimeters. The real dimension of the object is somewhere in the middle of the recovered values, where the diameter is 60mm and the aspect ratio 1.9. The difference in the dimension is reflected also in the magnetic moments, since the smaller objects have smaller magnetic moments. (*The total reduction in the residuals for the first test was about 47.3%, in the second test about 37.1% and in the third 25.7%*).

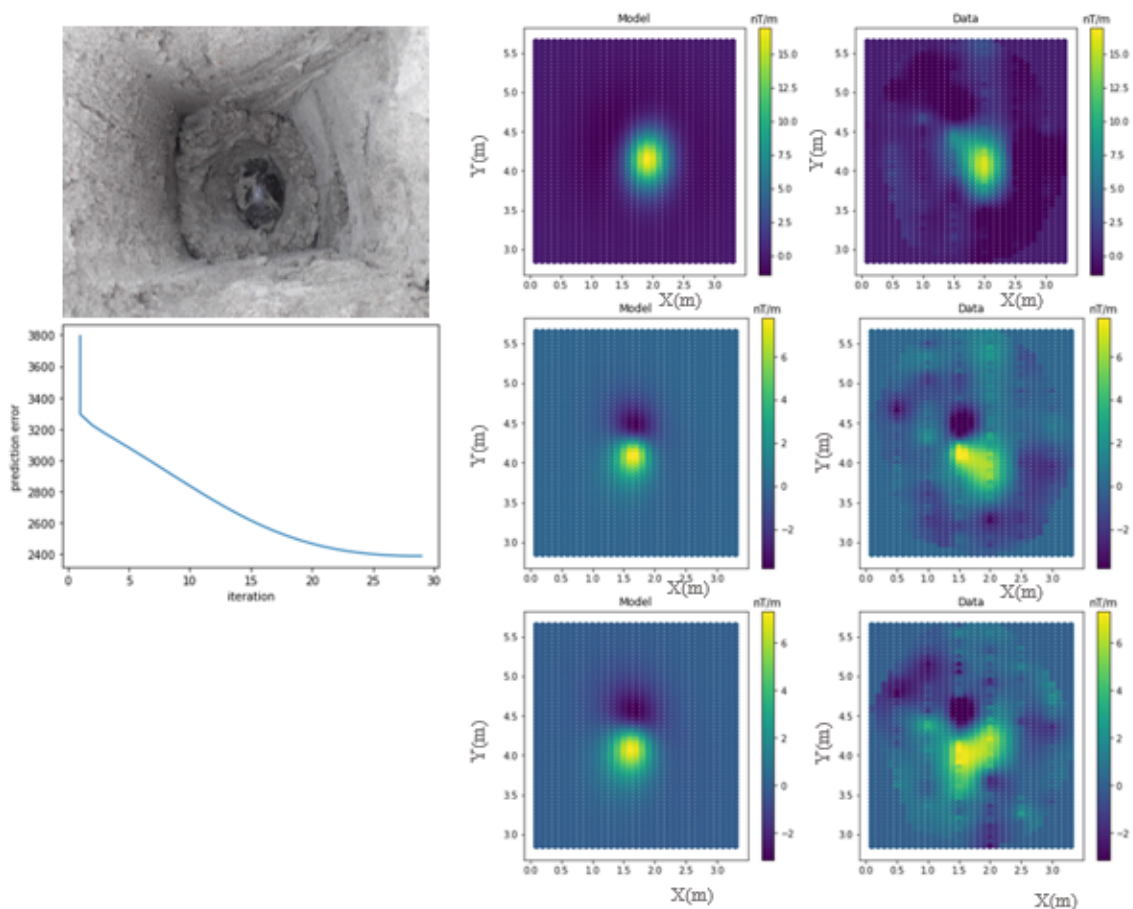


Figure 4.5: Inversion results for the hand grenade. The first figure on the top right is due to a vertical placed object, the one below is when the object is horizontal in the North-South direction and the last one is horizontal in the East-West direction. A plot on how the summed squared residuals act during the inversion is also included (for test 2).

4.2.3. CANNON BALL

The cannon ball acts like a sphere. Even though the orientation changes, the aspect ratio is not large enough to influence the induced field (fig. 4.6). The positions are rather similar with the real ones,

UXOS \ Hand Grenade	Test 1	Test 2	Test 3
Position [m]	x=1.90 y=4.17 z=0.62	x=1.70 y=4.22 z=0.39	x=1.68 y=4.23 z=0.49
$\phi, \theta [^\circ]$	34.9,-89.4	27.5,104.3	29.2,107.1
$\alpha [m], e [-]$	0.09,1.9	0.04,1.7	0.04,1.7
Magnetic moment [Am^2]	0.012	0.0002	0.00045
Residuals [nT/m]	3268.1	2389.7	2228.4

Table 4.2: Values of the recovered parameters for each test for the hand grenade. Note that the real values of the grenade are: $x = 2 \pm 0.2m, y = 4 \pm 0.2m, z = 0.6 \pm 0.2m, \alpha = 0.06$ m and $e=1.9$

within the expected uncertainty range. Similarly, the recovered depths from test 1 and 2 deviate only 4mm, while test 3 there is a slight bigger difference of 1 cm. The latter is possible to be due to errors in the pre-processing corrections or noise in the data (fig. 4.6 C). The angles are zero, since the three axis of the spheroid are close to equal. The calculated aspect ratios and diameters are similar to each other, but also close to the e of the object. That is also reflected in the recovered magnetic moments, although the slightly bigger recovered diameter of test 3 increased the moment by $0.018 Am^2$. (The total reduction of the residuals for each test was: 81.1%, 88.4%, 78.4%).

UXOS \ Cannon Ball	Test 1	Test 2	Test 3
Position [m]	x=2.06 y=7.90 z=0.56	x=2.06 y=7.85 z=0.56	x=2.03 y=8.09 z=0.70
$\phi, \theta [^\circ]$	0,0	0,0	0,0
$\alpha [m], e [-]$	0.07,1.2	0.07,1.2	0.08,1.2
Magnetic moment [Am^2]	0.031	0.031	0.049
Residuals [nT/m]	16965.6	10341.0	19475.2

Table 4.3: Values of the recovered parameters of each test for the cannon ball. Note that the real values of the Cannon ball are $x = 2 \pm 0.2m, y = 8 \pm 0.2m, z = 0.6 \pm 0.2m, \alpha = 0.10$ m and $e=1$

4.2.4. MORTAR

During the analysis of the mortar UXO, it was only possible to recover results for test 1 and 3. Modeling Test 2, which is where the object was placed at an angle with the horizontal was not feasible. The reason for that could lie in the pre-process or tail interference (usually not the case since most of them are made from aluminium) or the absence of the modelling of the remanent magnetization. Nevertheless, a horizontal orientation is enough to introduce a model that explains the anomaly produced by this specific UXO. The positions are comparable with the expected values, as well as their depths. Even though the objects are placed in a horizontal position, there is a small dip, around 12° in Test 1 towards the South. In test 3 the dipole moment is perpendicular with respect to the geomagnetic field, while the azimuth is 87.7° (or 2.3° from East). The comparatively larger residuals could be the result of the remanent magnetization, a phenomenon that is not accounted for in the code. Lastly, the dimensions of the body as well as their magnetic moments, yielded reasonable values. The deviations from the real parameters were 9.8 and 4.2mm for the diameter and 0.01 and 0.3 for the aspect ratio. The larger recovered diameter of test 1 led to a larger magnetic moment by $0.06 Am^2$ (Total reduction of the residuals for each test were: 72.9% for test 1 and 68.9% for test 3).

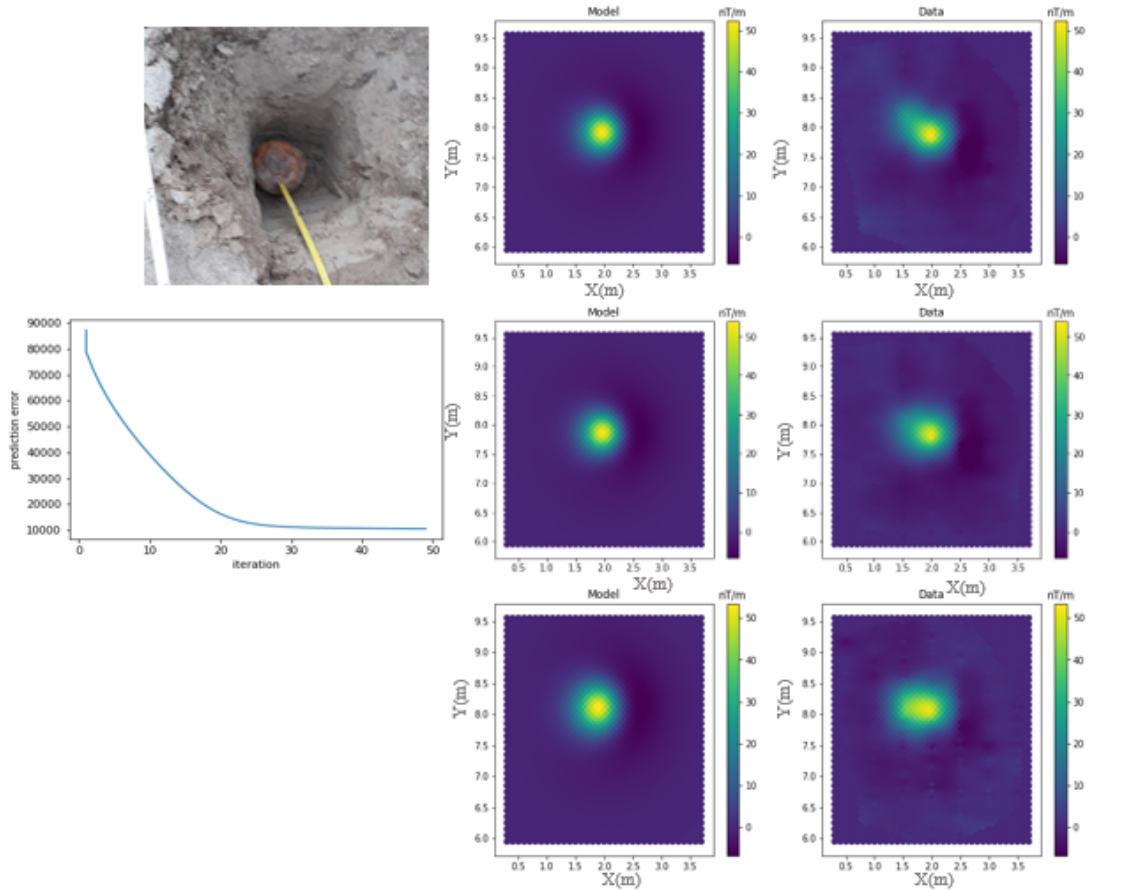


Figure 4.6: Inversion results for the Cannon Ball. Though in tests 2 and 3 the orientation of the ball is changed to a dipping manner towards the North and to a horizontal position in the East-West direction, no changes are visible in the maps. A plot on the behavior of the residuals is also included.

Mortar \ UXOS	Test 1	Test 2	Test 3
Position [m]	x=2.02 y=11.74 z=0.62	-	x=1.92 y=11.96 z=0.61
$\phi, \theta^{[o]}$	28.6,72.7	-	87.1,2.3
$\alpha[m], e[-]$	0.086,5.11	-	0.072,4.9
Magnetic moment [Am^2]	0.34	-	0.28
Residuals [nT/m]	311641.14	-	435266.10

Table 4.4: Values of the recovered parameters of the Mortar, for each test. It was not possible to acquire a model for the dipping object. Note that the real values of the mortar are: $x = 2 \pm 0.2m, y = 12 \pm 0.2m, z = 0.6 \pm 0.2m, \alpha = 0.076$ m and $e=5.2$

4.2.5. BRITISH SHELL

Modeling the British Shell was quite challenging. Test 1 and 3 overestimated the dimension of the of the target. Test 1 is almost horizontal, but exhibits a very small angle towards the North,. Test 2 shows a large inclination towards the North that is close to 60° . Test 3 is placed also in an almost horizontal position with an azimuth of 85.8° . (The total reduction of the residuals were: 88.9% or test 1, 88.95% for test 2 and 65.2% for test 3).

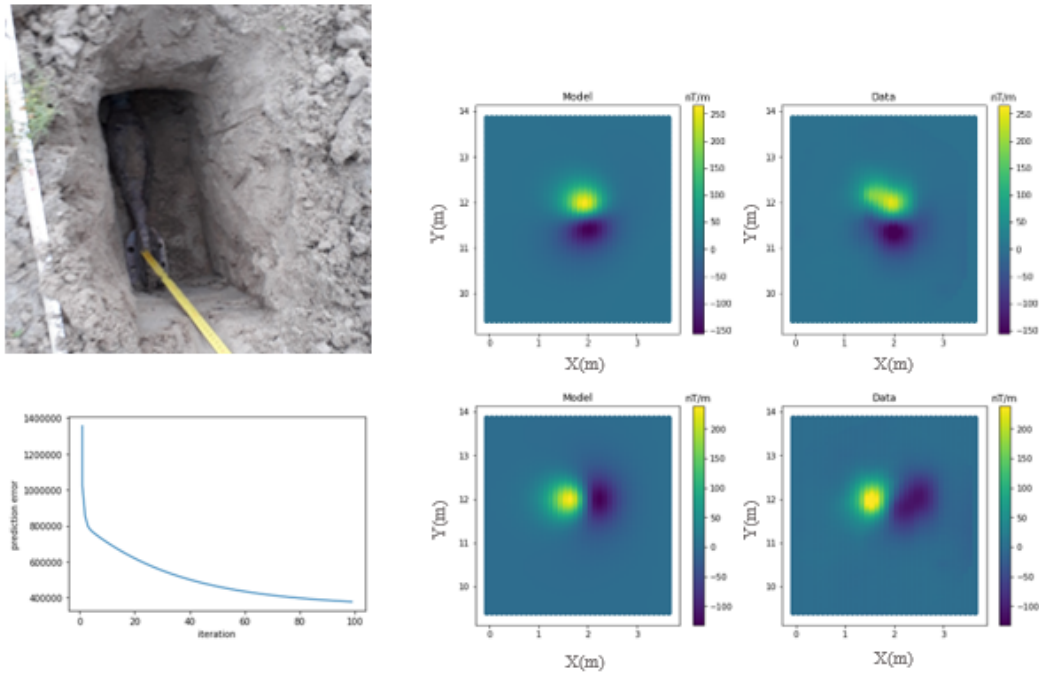


Figure 4.7: Anomaly maps for the Mortar UXO. The one at the top right is produced by a horizontally placed object in the North-South direction, while the one at the bottom right is from a horizontally placed in East-South direction object.

British Shell	Test 1	Test 2	Test 3
UXOS			
Position [m]	x=2.07 y=15.8 z=0.61	x=2.07 y=15.7 z=0.46	x=1.99 y=16.05 z=0.7
$\phi, \theta^{[o]}$	25.8,91.1	-14,-29.8	85.4,4.2
$\alpha[m], e[-]$	0.18,7.5	0.11,4	0.09,7.14
Magnetic moment [Am^2]	1.04	1.01	1.64
Residuals [nT/m]	1645431.	6406671.7	1914376.3

Table 4.5: Values of the recovered parameters for the British Shell UXO. Note that the real values of the british shell are $x = 2 \pm 0.2m, y = 16 \pm 0.4m, z = 0.6 \pm 0.2m, \alpha = 0.0876$ m and $e=3.7$

4.3. INVERSION RESULTS USING THE DIPOLE AND THE OCTUPOLE FIELD

The octopole term is decaying rapidly, about $\frac{1}{r^5}$. Figure 4.9 depicts the dipole and the octupole term of 105mm projectile for depths of one and two body lengths. Their magnitudes are normalized by the dipole magnitude. According to Butler et al. 2012 and Billings et al. 2002, when the depth and the body length ratio is one, then the octupole is 15% of the dipole magnitude. On the other hand, if the ratio is two, then the contribution is less than 5% of the dipole. All of the studied UXO's have a depth/length ratio over one and only the mortar and the British shell have a ratio less than two (1.5 and 1.8 respectively). Thus, the focus will shift to those two objects. The results are demonstrated below (table 4.6). It is obvious that the octupole does not have much effect on the results. In the Mortar case, there was a small improvement in the models shape, and consequently in the magnetic moment,

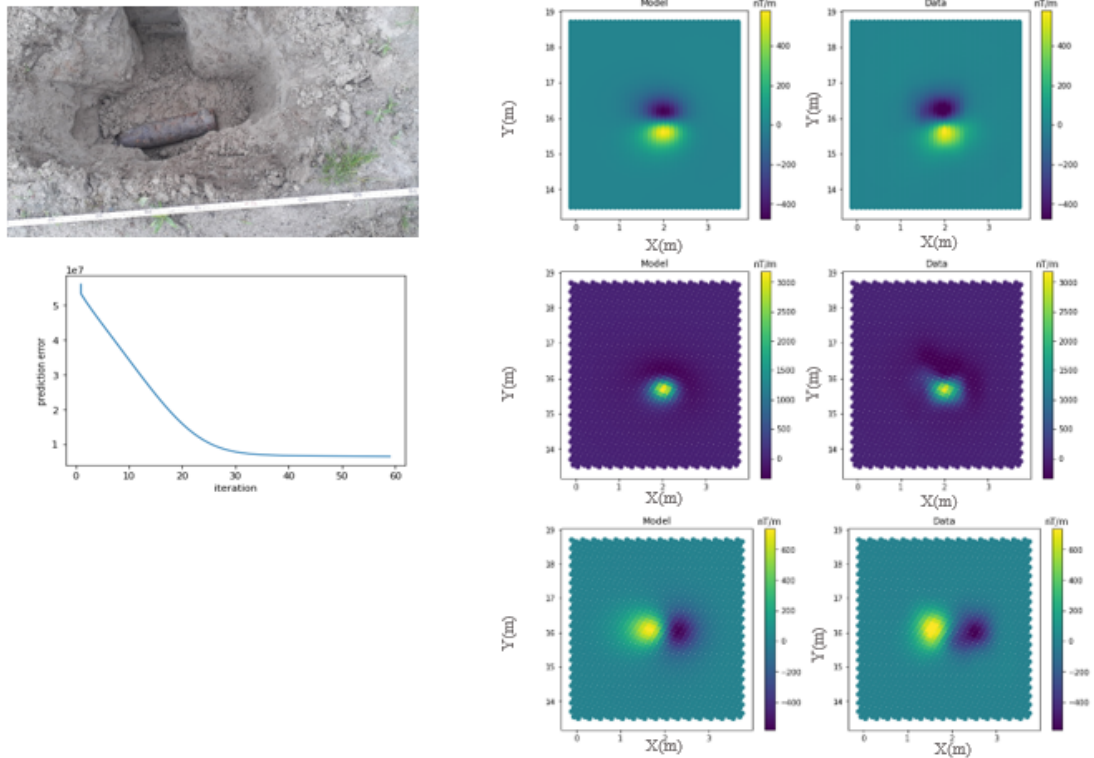


Figure 4.8: Inversion results for the British Shell UXO. The figure on the top right is generated by a horizontally place object at the direction of North-South, the one in the middle is from a dipping towards the North object and the last one is when the body is arranged in a horizontal manner but in the East-West orientation.

resulting in a small decrease of the residuals of about 57.54 nT/m (0.0005%). In the shell case there was not a lot of change in the dimensions of the model, apart of a small increase in the diameter and the angles, which led to an increase of 0.16 Am^2 in the magnetic moment. It also improved the position and especially the depth by 40mm. The decrease in the residuals was approximately 1589156 nT/m (or 2.65%).

	Test 1	Test 2
	Mortar	British Shell
Position [m]	x=2.02 y=11.74 z=0.62	x=2.62 y=15.74 z=0.50
ϕ, θ°	29.2, 72.8	-14.9, -30.4
$\alpha [m], e [-]$	0.086, 5.17	0.12, 4.0
Magnetic moment [Am^2]	0.35	1.27
Residuals [nT/m]	311583.6	4817515.7

Table 4.6: Inversion results, using the dipole and the octupole term for the mortar and the British shell. For the former test 1 was chosen, while for the latter test 2 was preferred, as it generated a more accurate model.

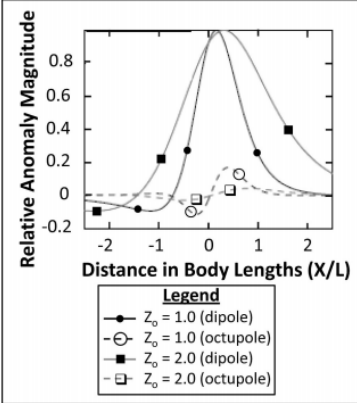


Figure 4.9: Plots of the dipole and octupole term for an 105mm projectile (length=0.389m and e=3.7.) (Billings et. al 2002)

5

DISCUSSION AND CONCLUSIONS

Overall the modeling of the spheroid was successful for the most of part. Inversions of the first UXO, as well as the grenade and the cannon ball, generated models that were close to measured object. The mortar and the British Shell produced models with greater residuals. According to Mcfee et al. 1989, deviations from reality are attributed to the remanent magnetization. This property is very difficult to model since its strength and direction are usually unknown. The common way of dealing with the remanent magnetization, is by simply ignoring modeling it. This does not cause major problems in the case that the object's history is not very complicated, such as in the first three inversions. On the other hand, we need to consider that normally, the chemical and thermal history of a UXO typically has seven stages. The first step concerns the conversion of the elemental iron to liquid steel and then into a raw steel bar. In the second stage, the bar is forged into a projectile, while in the fourth one, the object is fired (but not detonated). The fifth, the sixth and last phase include the storage, transportation and waste respectively. Physical and thermal variations can occur only in the first four stages. Thermoremanent magnetisation and working remanent magnetization can exist during the cooling down of the steel and the cold extrusion. During the impact, shock magnetization can also affect the direction of the magnetic domains [15]. Considering the above, it is rather challenging to predict how the remanent magnetization will influence the induced field and neglecting it, might introduce major errors in the interpretation of the results.

Another difficulty lies in the initial model that will be inserted into the code. A gradient solver, requires initial values, from which the minimization of the objective function will begin. If these values are not close to the real ones and the scaling is not adequate, then it is possible for the inversion to get stuck at a local minimum. This is partially solved by performing forward modeling. For most cases, the results were gratifying, except the British shell case. This case is an example where we have to evaluate the trade of between a lower misfit and a reliable model. Trying to minimize the objective function does not necessarily convey the right answer. Without prior knowledge of the object, it is possible to acquire a wrong model, within the range of uncertainty. That is called non-uniqueness and it is a fundamental phenomenon for all the potential geophysical methods. A convenient way to validate the spheroid model, is to compare it with the sphere. There was a high correlation between these models, especially for the magnetic moment and the depth. The best fit is always carried out by the sphere, though whether that can establish it as the best model, is difficult to judge. Especially since they are handling different parameters with different methods and having to decide between a better fit and a better model. To conclude, modeling a spheroid is a more complicated process than modeling a sphere, but way less troubling than considering a non-symmetric shape. Sometimes a sphere or spheroid model is not enough to explain the magnetic anomaly and thus more rigorous analysis is required. Even though the analytical solutions might contribute in understanding how the fields work, their practical use is limited in ferromagnetic objects. Remanent magnetization and complicated boundaries might require

direct solving of the differential or integral equations, by using advanced numerical techniques [5]. Including higher order moments can also attribute in better shape approximations. These methods are more complicated to achieve, but they can minimize the uncertainties and help identify and discriminate potential UXOs, in the most effective way possible.

A

APPENDIX A

This appendix contains more tests with synthetic results. The "real" model was the same as the one used in section 3.8. Table A.1 includes the initial model for each test.

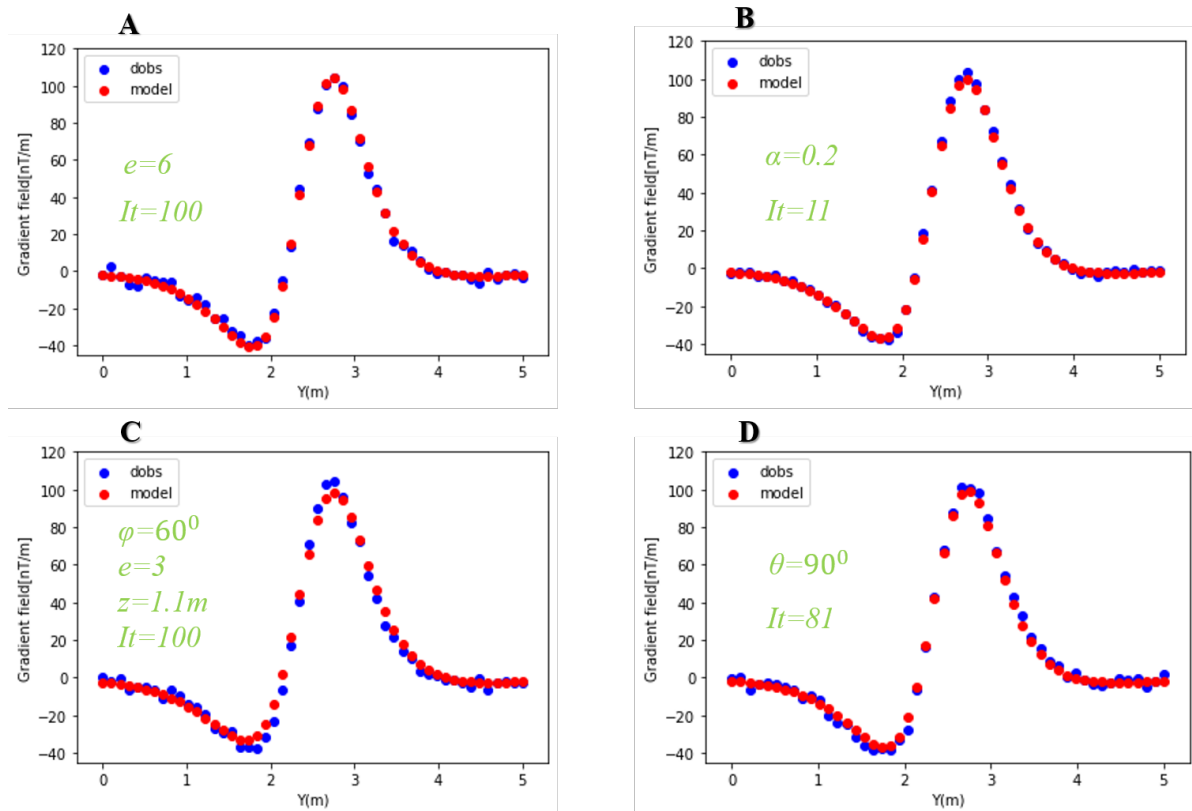


Figure A.1: Inversion tests with synthetic results, in order to evaluate the sensitivity of the parameters. Figure A represents results where only the aspect ratio was changed. The inversion converged at 100 iterations. Figure B shows results where the diameter was 0.2. The convergence was possible at 11 iterations. Figure C illustrates an inversion with multiple variables deviating from the real ones. The iterations were 100. Figure D reached convergence at 81 iterations, with varying variable being the theta angle. Detailed information about the "real" and initial models is contained in table A.1.

	Position (m)	ϕ, θ	α (m)	e (-)
"Real" model	x=2.5 y=2.5 z=1	45, 45	0.1	4
Initial Model A	x=2.5 y=2.5 z=1	45, 45	0.1	6
Initial Model B	x=2.5 y=2.5 z=1	45, 45	0.2	4
Initial Model C	x=2.5 y=2.5 z=1.1	60,45	0.1	3
Initial Model D	x=2.5 y=2.5 z=1	45,90	0.1	4

Table A.1: This table shows the initial values for each test. Note that B test contained noise with a zero mean and standard deviation of one, while A, D and C inversions were conducted with noise of standard deviation equal to two.

Bibliography

- [1] UNICEF. “Children and Landmines: A Deadly Legacy”. In: ().
- [2] Jennifer Dathan. *The environmental consequences of explosive weapon use: UXO*. 2020. URL: <https://aoav.org.uk/2020/the-environmental-consequences-of-explosive-weapon-use-uxo/>.
- [3] Dwain K. Butler. “Potential fields methods for location of unexploded ordnance”. In: *Geophysics* 20 (Aug. 2001). DOI: 10.1190/1.1487302.
- [4] Vinicio Sanchez et al. “Relative importance of magnetic moments in UXO clearance applications”. In: *Seg Technical Program Expanded Abstracts* 25 (Jan. 2006). DOI: 10.1190/1.2369777.
- [5] John E. Mcfee. *ELECTROMAGNETIC REMOTE SENSING LOW FREQUENCY ELECTROMAGNETICS*. 124th ed. Defence Research Establishment Suilfield Ralston AB, Canada TOJ 2NO, 1989.
- [6] Harsh Bhatia et al. “The Helmholtz-Hodge Decomposition—A Survey”. In: *IEEE Transactions on Visualization and Computer Graphics* 19.8 (2013), pp. 1386–1404. DOI: 10.1109/TVCG.2012.316.
- [7] Christopher S. Baird. “Helmholtz Decomposition of Vector Fields”. In: ().
- [8] Williams Lowrie. *Fundamentals of Geophysics*. New York: Cambridge University Press, 2007.
- [9] Dwain K. Butler et al. “Review of Magnetic Modeling for UXO and Applications to Small Items and Close Distances”. In: *Journal of Environmental and Engineering Geophysics* 17 (June 2012), pp. 53–73. DOI: 10.2113/JEEG17.2.53.
- [10] Robert C. O’Handley. *Modern magnetic materials: Principles and applications*. New York: John Wiley, 2000.
- [11] Stephen Billings, Leonard Pasion, and Douglas Oldenburg. “Discrimination and Identification of UXO by Geophysical Inversion of Total-Field Magnetic Data”. In: (Sept. 2002), p. 58.
- [12] Janet Simms, Remke Van Dam, and Jan Hendrickx. “Classification of magnetic susceptibility anomalies and their relevance to UXO detection”. In: *Fast Times* 10 (Jan. 2005), pp. 48–51.
- [13] Qianqian Chen. “Localizing a magnetic dipole using a gradiometer”. In: (2020).
- [14] Simon P. Neill and M. Reza Hashemi. “Chapter 8 - Ocean Modelling for Resource Characterization”. In: *Fundamentals of Ocean Renewable Energy*. Ed. by Simon P. Neill and M. Reza Hashemi. E-Business Solutions. Academic Press, 2018, pp. 193–235. ISBN: 978-0-12-810448-4. DOI: <https://doi.org/10.1016/B978-0-12-810448-4.00008-2>. URL: <https://www.sciencedirect.com/science/article/pii/B9780128104484000082>.
- [15] W. Goodrich. “Characterization and quantification of magnetic remanence in unexploded ordnance”. In: 2007.